Nanoparticle-Functionalized Polymer Platform for Controlling Metastatic Cancer Cell Adhesion, Shape, and Motility

Hyojin Lee,[†,‡] Yeongseon Jang,[†,§] Jinhwa Seo,[§] Jwa-Min Nam,[‡,*] and Kookheon Char[§,*]

[‡]Department of Chemistry, Seoul National University, Seoul, 151-747, Korea and [§]School of Chemical and Biological Engineering, The National Creative Research Initiative Center for Intelligent Hybrids, The WCU Program of Chemical Convergence for Energy & Environment, Seoul National University, Seoul, 151-744, Korea. [†]These authors contributed equally to this work.

ABSTRACT Controlling and understanding the changes in metastatic cancer cell adhesion, shape, and motility are of paramount importance in cancer research, diagnosis, and treatment. Here, we used gold nanoparticles (AuNPs) as nanotopological structures and protein nanocluster forming substrates. Cell adhesion controlling proteins [in this case, fibronection (Fn) and ephrinB3] were modified to AuNPs, and these particles were then modified to the layer-by-layer (LbL) polymer surface that offers a handle for tuning surface charge and mechanical property of a cell-interfacing substrate. We found that metastatic cancer cell adhesion is affected by nanoparticle density on a surface, and ~140 particles per 400 μm^2 (~1.7 μm spacing between AuNPs) is optimal for effective metastatic cell adhesion. It was also shown that the AuNP surface density and protein nanoclustering on a spherical AuNP are controlling factors for the efficient interfacing and signaling of metastatic cancer cells. Importantly, the existence of nanotopological features (AuNPs in this case) is much more critical in inducing more dramatic changes in metastatic cell adhesion, protrusion, polarity, and motility than the presence of a cell adhesion protein, Fn, on the surface. Moreover, cell focal adhesion and motility-related paxillin clusters were heavily formed in cell lamellipodia and filopodia and high expression of phospho-paxillins were observed when the cells were cultured on either an AuNP or Fn-modified AuNP polymer surface. The ephrin signaling that results in the decreased expression of paxillin was found to be more effective when ephrins were modified to the AuNP surface than when ephrinB3 was directly attached to the polymer film. The overall trend for cell motility change is such that a nanoparticle-modified LbL surface induces higher cell motility and the AuNP modification to the LbL surface results in more pronounced change in cell motility than Fn or ephrin modification to the LbL surface.

KEYWORDS: nanoparticle · layer-by-layer polymer substrate · metastatic cancer · fibronectin · ephrin

Metastasis is typically initiated by the detachment of cancer cells from a primary tumor site, and this process may require the decreased adhesiveness to tumors or a stromal matrix. The arrest in the target organ that results in tumor-specific patterns of metastasis formation may be mediated by specific tumor−endothelial interactions and selective binding to specific matrix components.[1,2] In this regard, understanding and controlling the adhesion behavior of metastatic cancer cells is of paramount importance to cancer research and treatment. Many recent cell research results suggest that cells need to be cultured with proper biological molecules and cell-adhering environments to generate *in vivo*-like results. For these studies, engineered biomaterials mimicking *in vivo* extracellular environments have been widely investigated and applied to various cell research and cell/tissue engineering applications.[3−6] Among them, the layer-by-layer(LbL)-assembled structures[7,8] are promising platforms that offer ways to generate complex physical, chemical, and biological properties in a straightforward fashion.[7,9−13] Surface properties such as hydrophilicity,[14] charge density,[9] and film rigidity[15,16] could be easily tailored by the adjustment of the chemical nature of polyelectrolytes, pH, temperature, and the number of bilayers. Moreover, the LbL films are capable of incorporating biomolecules such as cell adhesion proteins and peptides[11,17,18] as well as functional inorganic materials such as nanoparticles. Recently, it has been reported that the cellular behaviors are affected by the nanofeatured substrates modified with nanoparticles,[19,20] and advances in the nanofabrication method allow studying the effect of the nano/microenvironment on the cell culture and assay of interest.[21−26] The cells have often been independently investigated for either the effect of biological molecules or the ligand clustering and cell membrane curvature controlled by nanoenvironments.[27−31] It is, however, obvious that biomolecular recognition/signaling and nanoenvironment concomitantly and cooperatively influence cells to generate natural phenotypes.

Herein, we designed and fabricated biomolecule and nanoparticle-functionalized

* Address correspondence to jmnam@snu.ac.kr; khchar@plaza.snu.ac.kr.

Received for review February 12, 2011 and accepted June 24, 2011.

Published online June 24, 2011
10.1021/nn202103z

LbL polymer platforms to study and control the phenotypic changes of breast metastatic cancer cells (CAMA-1) (*i.e.*, focal adhesion, spreading, surface projections, and so forth). The response of the metastatic cancer cells to the surrounding environment could be different from normal or nonmetastatic cancer cells, and they have not been studied in detail with nanoenvironments. Importantly, human breast metastatic cancer cells (CAMA-1) have not been fully understood in terms of their adhesion and migration on extracellular matrix (ECM) as well as the interactions with AuNPs. AuNPs are useful nanostructural components in cell study because the surface of AuNPs is readily modifiable with various biomolecules.[32] Furthermore, AuNPs exhibit very low or no cytotoxicity, and AuNPs have widely been used not only for cell adhesion studies[33−35] but also for *in vivo* thermal therapy,[36] drug delivery,[37] and tumor targeting.[38] To observe the phenotypic changes of CAMA-1 cells interacting with AuNPs in the present study, nanofeatured surfaces were realized by immobilizing pristine AuNPs or biomolecule-modified AuNPs on LbL polymer substrates. We used fibronectin (Fn) and ephrin as cell adhesion controlling biomolecules as either free forms or AuNP-conjugated forms. Fn, an ECM protein, is a cell adhesive molecule that can specifically bind to the integrin of a cell surface. Accordingly, Fn-conjugated AuNPs could serve as ECM adhesion sites. On the contrary, it has been shown that ephrin-Eph receptor signaling decreases cell adhesion[39] and guides cancer metastasis, and elevated ephrinB3 expression was reported in invasive glioma cells.[40−42] This ephrin-Eph receptor communication sends signals to the receptor tyrosine kinase of Eph receptors, which affects the metastatic cellular activities including the expression of actin cytoskeleton, adhesion to surface, intercellular junctions, and morphological changes. Finally, a positively charged polymer surface, constructed by the spin-assisted LbL deposition method yielding a well-ordered thin film with uniform surface charge, could tightly immobilize negatively charged Fn and ephrinB3 or AuNPs on the surface. In addition, the LbL surface platforms act as hydrated polymer cushions to passivate artificial glass substrates and also offer plenty of targeted functionalities, in contrast to bare glass substrates, to study the effect of biological and physicochemical cues on the cellular behavior.[43,44] Using these versatile biomolecule- and nanoparticle-functionalized LbL platforms, we assembled both cell−ECM and cell−cell interaction systems on polymer substrates and investigated the effect of nanofeatures as well as biological recognition on the cell behavioral changes in adhesion, cytoskeletal organization-based morphology, and motility of human breast metastatic cancer cells (CAMA-1).

RESULTS AND DISCUSSION

Preparation and Characterization of Nanoparticle-Functionalized Polymer Matrixes. In a typical experiment, nanoparticle-functionalized polymer matrixes were prepared as schematically depicted in Figure 1. The polymer films were prepared on the basis of the spin-assisted LbL deposition method[45] to build various substratums in a straightforward fashion. These polymer films can serve as hydrated polymer cushions to hinder the artificial solid glass substrate effect and allow for adjustable cellular interactions.[46] Poly(allylamine hydrochloride) (PAH) and poly(acrylic acid) (PAA) were employed as the basic building blocks for polyelectrolyte matrixes, and the PAH layer is the top layer that presents positive charges. Negatively charged pristine AuNPs or AuNPs conjugated with Fn or ephrinB3 are tightly bound to the positively charged LbL films placed on the glass substrates. The Fn or ephrinB3 is electrostatically conjugated to the surfaces of 50 nm AuNPs. We calculated the amount of modified protein per AuNP by comparing total protein amount in solution before and after AuNP addition using the Bradford assay, as summarized in Table S1 (see Methods and Supporting Information for detailed information). These biomolecule-conjugated AuNPs were then spread on the LbL polymer surfaces using the spin-assisted deposition method, which usually offers more uniform internal structure and surface of multilayer films when compared with the conventional dip-assisted deposition method. Zeta potential measurements indicate that the citrate-, Fn-, and ephrinB3-conjugated AuNP/LbL surfaces are all negatively charged (Figure 2a; all the particles were spread on positively charged PAH surfaces through the electrostatic interaction, and it should be noted that the ephrinB3-conjugated AuNP/LbL surface displayed the highest negative charge). The surface morphology and hydrophilicity of the prepared matrixes were characterized by an atomic force microscope (AFM) and water contact angle measurements, respectively (Figure 2a). AuNP-modified LbL surface, Fn- or ephrinB3-AuNP-conjugated LbL surface, and Fn- or ephrinB3-coated LbL surface without AuNPs are denoted as AuNP/LbL, Fn-AuNP/LbL, ephrinB3-AuNP/LbL, Fn/LbL, and ephrinB3/LbL surfaces, respectively. Spin-coated AuNPs were randomly distributed on the LbL films, as shown in Figure 2a. Water contact angle experiments show that the LbL polymer surface displayed the lowest hydrophilicity, and the Fn-AuNP/LbL polymer surface showed the highest hydrophilicity. Compared to a bare LbL film, the surface roughness and hydrophilicity of AuNP/LbL, Fn-AuNP/LbL, and ephrinB3-AuNP/LbL films were slightly increased, respectively, due to the introduction of hydrophilic nanoparticles to the surface. It is possible for cells to take up particles from the surface, and this should be avoided in our case because

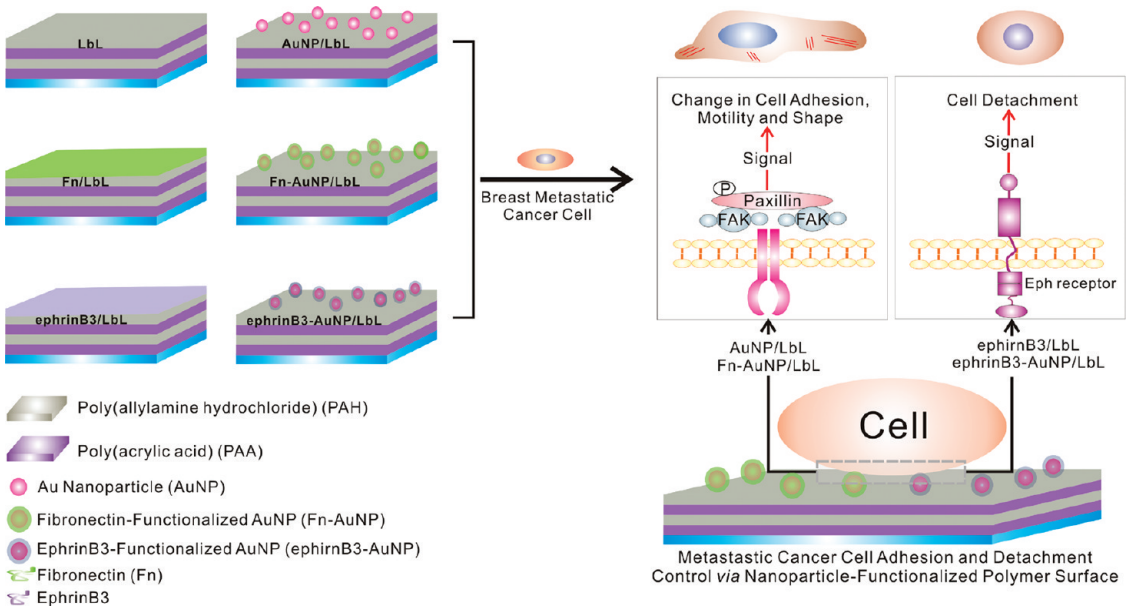

Figure 1. Schematic of metastatic cancer cell assay on nanoparticle-functionalized polymer platform. AuNPs, protein-conjugated AuNPs (Fn-AuNP or ephrinB3-AuNP), or proteins (Fn or ephrinB3) were introduced on the surface of the layer-by-layer assembled $(PAH/PAA)_{5.5}$ LbL films. CAMA-1 human breast epithelial metastatic cancer cells were cultured and analyzed on the functionalized polymer surfaces.

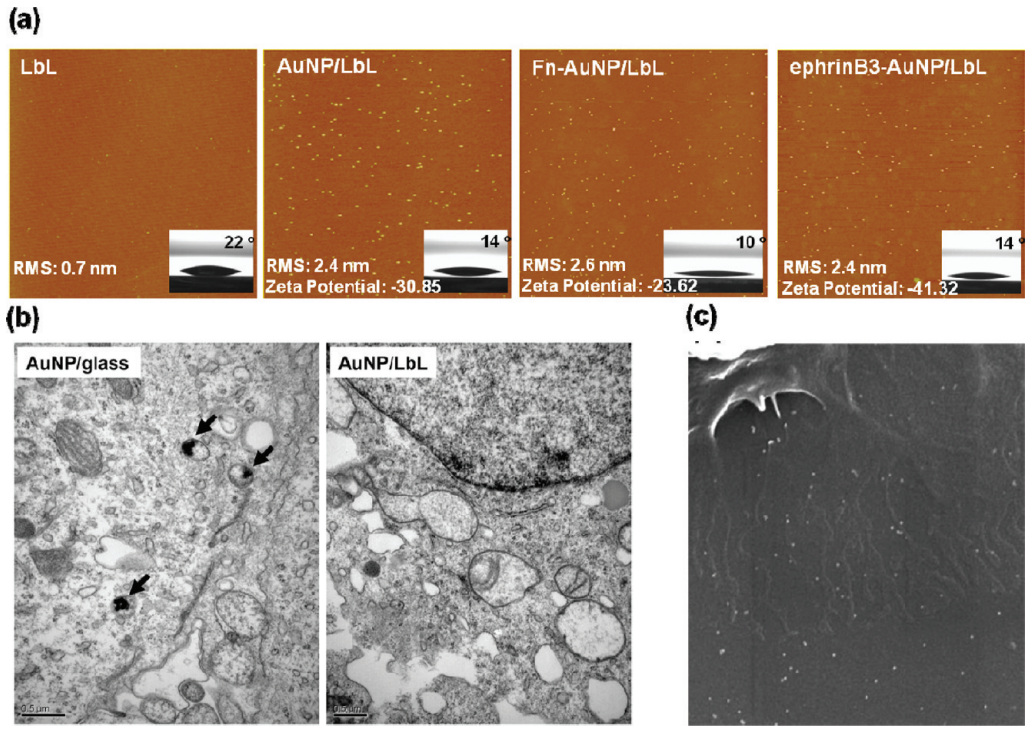

Figure 2. (a) AFM height images of the LbL, AuNP/LbL, Fn-AuNP/LbL, and ephrinB3-AuNP/LbL substrates, respectively (scan area: 20 μm $\times$ 20 μm). The insets in all figures show water contact angles of each surface. The values for zeta potential and RMS for surface roughness are also shown. (b) TEM images of CAMA-1 cells after 2 days of culture on AuNP-coated bare glass (AuNP/glass) and AuNP/LbL substrate. The scale bars in both images are 500 nm. The uptake of AuNPs within CAMA-1 cells is detected in the case of AuNP/glass (see the arrows in the left image), while no AuNPs were detected for the AuNP/LbL substrate. (c) SEM image of the lamellipodia of a CAMA cell on the AuNP/LbL substrate. CAMA-1 cells were cultured on the AuNP/LbL substrate with a density of 300 AuNPs in a 400 μm^2 area for 2 days.

here we need to use nanoparticles as cell-interfacing nanofeatures on the surface. We tested whether AuNPs residing on the LbL film surface can be taken up by metastatic cancer cells after incubation in a cell culture medium (two cases were tested herein; AuNPs on a bare glass surface and on a LbL polymer surface,

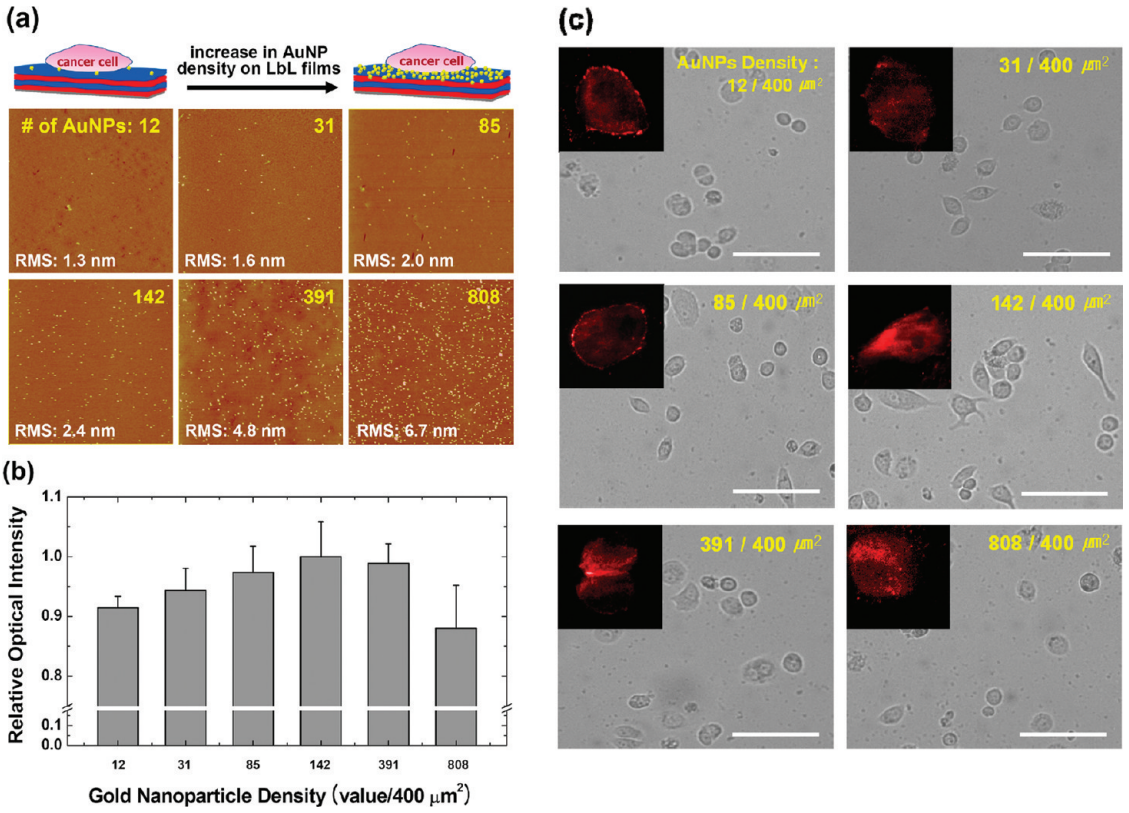

Figure 3. Cell adhesion study on AuNP density-controlled polymer surface. (a) AFM images of AuNP/LbL surface (area: 20 μm × 20 μm) with varying AuNP densities. The numbers in all the images show the number of AuNPs within a 400 μm^2 area, and the RMS surface roughness is also shown. (b) Relative paxillin amounts in CAMA-1 cells cultured on each sample obtained by the ELISA analyses. (c) Optical images of CAMA-1 cells cultured for 2 days on substrates with varying AuNP densities in DMEM with 10% FBS. Inset images are the total internal reflection fluorescence (TIRF) images of paxillin. The scale bars in all the images are 100 μm.

respectively). After two days of culture in DMEM medium with 10% FBS (37 °C, 5% CO_2 condition), cells were observed by TEM (LIBRA120, Carl Zeiss, Germany). No particles were found when the particles were attached to the LbL polymer surface through the electrostatic interaction, whereas AuNPs were found in the cytosol when the AuNPs were directly contacted on a bare glass surface (Figure 2b). These results show that the electrostatic interactions between AuNPs and the LbL polymer surface are necessary and strong enough to hold the particles on the surface when cells were interfaced with the particles in a cell culture medium (Figure 2b). Additionally, large and spreading lamellipodia were observed on the AuNP/LbL substrate (300 AuNPs/400 μm^2) after 48 h cell culture (Figure 2c). This SEM result shows the effective cell adhesion to an AuNP-modified surface without Fn and the high stability of the modified AuNPs on the LbL polymer surface.

Effect of AuNP Density on Breast Metastatic Cancer Cells. A series of substrates with different nanoparticle densities on the LbL films were prepared to investigate the change in metastatic cell adhesion in response to the change in nanoparticle density as well as surface roughness. For the nanotopological modification of LbL films, AuNPs, Fn-AuNPs, and ephrinB3-AuNPs in water (80 μL) were added to the PAH top-layered LbL film and spun at 3000 rpm for 20 s until a sufficiently dried film was obtained (an AuNP stock solution was prepared in deionized (DI) water at a concentration of 4.5 × 10^{10}/mL). In order to vary the density of AuNPs on the LbL film, we varied the repetition number of spin coating using the AuNP stock solution and diluted the AuNP stock solution with DI water. The AuNP densities of all the samples used in the cell culture were measured with the AFM images in >3 different regions. The detailed methods and results are shown in Table S2 (Supporting Information). The AuNP density on the surface was varied and correlated with cell adhesion. As the AuNP density on the LbL film surface was increased, the surface roughness increased accordingly. The RMS roughness value increases from 1.3 nm for 12 AuNPs/400 μm^2 up to 6.7 nm when more than 808 AuNPs/400 μm^2 were attached on the LbL film (Figure 3a). CAMA-1 cells (1 × 10^4 cells) were cultured on the AuNP/LbL substrates (81 mm^2) at different Au densities for 48 h. Cell morphology and paxillin distribution in cells, cultured on different substrates in 10% FBS with DMEM, were observed by an optical microscope after 48 h cell culture (Carl Zeiss Axiovert 200M) (Figure 3c). Interestingly, cell shape was dramatically changed to have the most polarized morphology for the 142 AuNP density condition. However, cells

maintained rather spherical morphologies on the substrates with lower or higher AuNP densities than 142 AuNPs/400 μm^2. Paxillin sandwich ELISA experiments were performed to analyze and quantify the cellular focal adhesion on a respective matrix. Paxillin is a focal adhesion-associated, phosphotyrosine-containing protein that plays roles in several signaling pathways such as the focal adhesion kinase (FAK)-Src signaling. When the focal adhesion of cultured cells is formed, a non-receptor protein tyrosine kinase (*i.e.*, FAK) is extensively expressed. FAK is activated by tyrosine phosphorylation when the integrin within the cell membrane is clustered during the cell adhesion or antibody cross-linking. FAK expression can enhance the cell spreading and migration.[47] In this mechanism, paxillin can recruit other cell adhesion-associated molecules and control the organization of the actin cytoskeleton and the rate of adhesion formation.[48] Therefore, this protein plays an important role in cell adhesion and cell migration process.[49] Overall, the amount of paxillin increases as the particle density is increased (Figure 3b). However, when the AuNPs were too densely coated on the polymer surface (>391 particles/400 μm^2), the amount of paxillin started to decrease. This result suggests that there exists a certain range in surface roughness for metastatic cancer cells to effectively adhere to the surface, and the cell adhesion could even be aggravated when too many nanoparticles are introduced to the cell adhesion surface. Cells usually respond differently to substrates under various conditions including varying geometry and topography.[50] It is well known that micrometer-scale roughness has an influence on cell proliferation and morphology. The protein clustering in focal adhesion of a cell, which is in the range 5−200 nm,[51] could be influenced by nanometer scale features, and the clustering of integrins has shown to play a critical role in the cell adhesion process as well as the focal adhesion of a cell. Spatz *et al.* demonstrated that cells responded differently to hierarchically structured adhesive nanopattern surfaces. They fabricated nanostructured surfaces using diblock copolymer and c(-RGDfK-)-thiol peptide-functionalized 6 nm AuNPs, which were arranged on differently sized square patterns. Cell responses including actin-associated, paxillin-rich focal adhesion and increase in paxillin domain length on AuNP arrays were observed.[52]

In our case, as the particle density on the polymer surface is decreased, the spacing between AuNPs becomes larger, and it is likely that the clustering of integrins is limited by the sparsely dispersed binding sites.[53] This is why particle density needs to be high for cells to bind to the surface. On the other hand, when the density of AuNPs on a polymer surface is too high and AuNPs are placed very close to each other, cells need to make an effort to reach the bottom of the substratum through the closely spaced particles and have many convexities of the cell membrane, each with a very small curvature radius.[54] These could cause a stressful condition in cell adhesion and proliferation, and cells try to minimize the contact area with the substrate to reduce the stress.[55] These factors could induce a negative effect on cell focal adhesion, and, consequently, a decreased paxillin amount could be observed for metastatic cancer cells on a substrate with a very high AuNP density. Our results suggest that the optimal AuNP density for the metastatic cell adhesion is ~140 particles per 400 μm^2 of the surface area. The average distance between AuNPs at optimal density is nearly 2 μm in this case, which is very large compared to the previous studies with other cells such as osteoblast cells. For osteoblast cells with other substrates, distances of more than 100 nm reduced integrin clustering.[53,56] They demonstrated the effect of nanopattern on osteoblast cell adhesion using ~10 nm AuNPs. They also used M-PEG-Si$(OMet)_3$ to prevent nonspecific cell adhesion. Our system is simply different from these cases. First, in our case, we used 50 nm AuNPs, which have a different surface geometry and lager surface area than 10 nm AuNPs. Second, we used layer-by-layer polymer substrate in this case. In our previous publication,[43] we showed that a positively charged PAH-top-layered layer-by-layer polymer substrate can play important roles in cell adhesion and morphology change. Finally, we did not use osteoblast cells here, but we used human breast metastatic cancer cells. We studied metastatic cancer cells that have a lower number of integrins on their cell surfaces than normal cells, and it was shown that CAMA-1 cells do not express cell adhesion-related integrin β4.[57−59] For these reasons, this lower nanoparticle density could be optimal for our system.

Observation and Analysis of Breast Metastatic Cancer Cells on Substrates. To investigate the metastatic cancer cell adhesion and morphology on the biologically functional nanoparticle surface, CAMA-1 cells (human breast epithelial metastatic cancer cells) were cultured in a DMEM medium with 10% FBS (37 °C, CO_2 5% condition, 1×10^4 cells/mL) on AuNP/LbL, Fn-AuNP/LbL, and ephrinB3-AuNP/LbL substrates for 2 or 7 days, respectively. The same cells were also cultured on bare glass and LbL film substrates with and without biomolecules (*i.e.*, LbL, Fn/LbL, and ephrinB3/LbL substrates) as control experiments.

The role of Fn for cancer cell adhesion is different depending on the type of cell line and environment, and it is interesting to see how Fn works on metastatic CAMA-1 cells when these Fn molecules are coated on nanoparticle surfaces. It is also likely that soluble Fn molecules exist in the medium, and these Fn in solution could deposit on the surface. However, the Fn-premodified surfaces should offer a different environment for cells from the surfaces postmodified with soluble Fn in solution. To find out cell culture medium effects on assay outcomes, 2-day cell-culture assay results in DMEM with 10% fetal bovine serum (FBS) were compared to the assay results in DMEM media without FBS or DMEM with 10% newborn calf serum

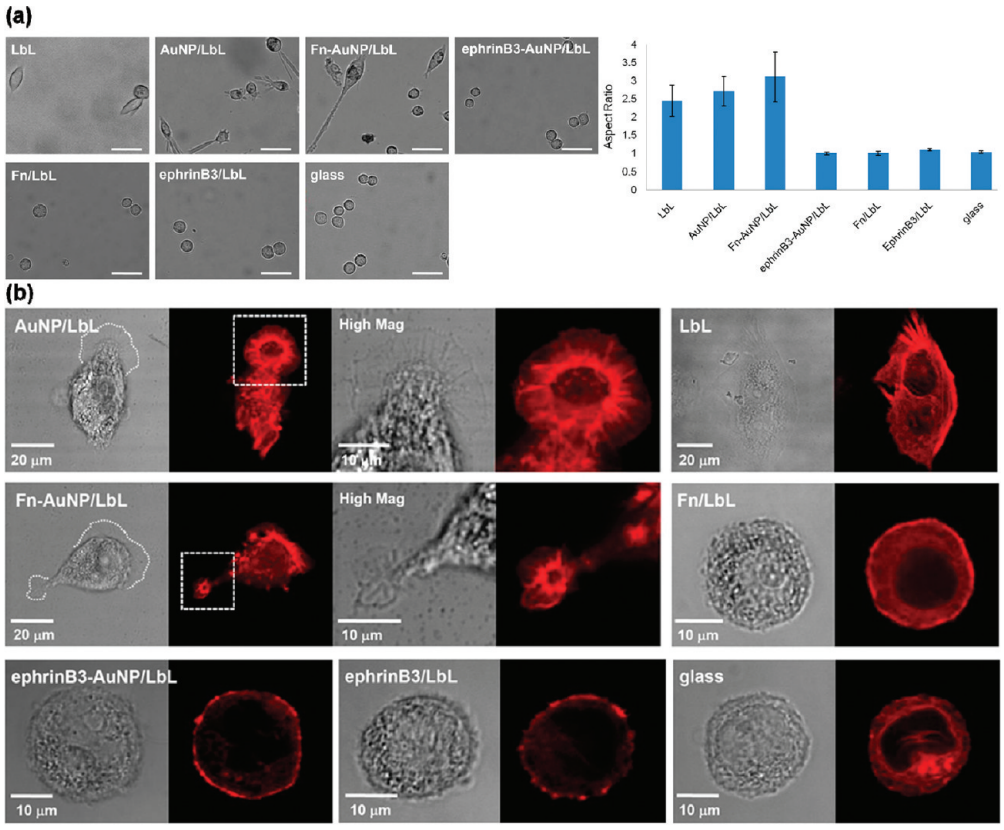

Figure 4. (a) Optical images of CAMA-1 metastatic cancer cells after 2 days of culture on glass, LbL, or fibronectin- or ephrinB3-coated LbL films and three different Au nanoparticle (AuNP, Fn-AuNP, or ephrinB3-AuNP)-coated LbL films. The scale bars in all the images are 50 μm. The graph on the right shows the varying average aspect ratio of CAMA-1 cells after 2 days of culture. (b) Optical images of actin-stained CAMA-1 metastatic cancer cells after 2 days of culture on various substrates. DIC and red fluorescence images were obtained at the same position of the cultured CAMA-1 cells. The third and fourth images in the first and second rows show the magnified images of the white dotted square areas in the second images of each row.

(NCS), respectively. It should be noted that FBS-free medium does not contain any proteins, and the NCS contains 2−3-fold more proteins, including Fn and immunoglobulin, than the FBS. The resulting data (Figures S2 and S3) showed that cellular responses to each substrate are similar in all three different medium conditions: remarkable cellular protrusions and polarization were observed from the spreading CAMA-1 cells on both AuNP/LbL and Fn-AuNP/LbL surfaces, as shown in Figure 4a, while no clear cell surface projections and polarization were observed for the Fn-LbL, LbL, and glass substrates. The results indicate that cellular morphology changes are indeed mainly due to changes in cell-interfacing surface structure and components.

To observe the cellular behavior at the early adhesion stage, we cultured cells in a chamber slide system (Live Cell Instrument, Cu-104) maintaining 37 °C and 5% CO_2. Cell adhesion occurs in three stages: (1) weak adhesion stage: cells initially contact a substrate, (2) intermediate adhesion stage: cells spread on the surface, and (3) strong adhesion stage: cells make stress fibers and form focal adhesions.[60] During the early adhesion stages (weak and intermediate adhesion), CAMA-1 cells actively recognize their local environment and make cellular protrusions of cell membranes on the AuNP/LbL and Fn-AuNP/LbL substrates (Figure S4). In the cell−substrate interactions, cells tend to increase their contact surface area, actin microfilament production, and cell spreading. Membrane ruffling such as lamellipodia and filopodia could induce strong adhesion of cells *via* the polymerization and depolymerization of actins.[61]

The morphological changes of breast metastatic cancer cells after 2 or 7 days of culture were observed and analyzed by an optical microscope (Carl Zeiss Axiovert 200M), and these optical images were used to calculate the aspect ratio of cells captured in the images of each sample for the quantitative analysis of cell morphological changes (Figure 4a and Figure S5). To further demonstrate the effect of the nanotopological surface on the cellular cytoskeletal organization and expression, the actin of CAMA-1 cells was stained with fluorescently labeled phalloidin-TRITC and analyzed under a confocal microscope (Leica TCS SP5) (Figure 4b). In the case of the PAH-top-layered LbL substrate without AuNPs (*i.e.*, LbL), CAMA-1 cells were attached to the positively charged LbL surface and

showed elliptical morphology, which is in good agreement with our previous results.[60] However, cell surface projection features (*e.g.*, lamellipodia and filopodia) were not clearly observed, and this indicates that the cells on this surface may not be highly mobile. The cells that we examined here are from a metastatic cancer cell line that is often less sticky to the surface when compared with normal or nonmetastatic cells. A recent paper stated that metastatic cancer cells have a fewer number of integrins on their cell surfaces or low adhesion between integrin and fibronectin compared with normal or cancer cells even when expressing comparable levels of integrins.[57] The surface of a metastatic malignant neoplasm cell displays a higher phosphatidylcholine/phosphatidylethenolamine ratio than that of malignant neoplasm cells with a low number of metastases.[62] The increased amount of the phosphatidylcholine phospholipids induces a more negatively charged surface of the metastatic cell membrane at the pH of a typical cell medium. This could explain why the metastatic CAMA-1 cells exhibit a spreading morphology even with fewer integrins on the cell surface on the positively charged LbL polymer surface while they do not show such morphology on the glass surface. Remarkable cellular protrusions were observed from the spreading CAMA-1 cells on both AuNP/LbL and Fn-AuNP/LbL surfaces, as shown in Figure 4a and b, while no clear cell surface projections were observed for Fn/LbL, LbL, and glass substrates. The cells on the AuNP/LbL and Fn-AuNP/LbL surfaces show significantly elongated anisotropic morphologies compared to those on the LbL substrate. CAMA-1 cells formed many large lamellipodia and filopodia that protrude out from the cell surface on the AuNP/LbL and Fn-AuNP/LbL substrates. We note that cells also take high aspect ratios on the AuNP/LBL and Fn-AuNP/LbL substrates, as evidenced in Figure 4a. These results agree quite well with the DIC images and fluorescence image results, and this overall trend of the cell morphological change was the same after 7 days of culture (Figure S5). Importantly, actin-staining results show that the strong actin bundle formation is involved with cell spreading on the AuNP/LbL and Fn-AuNP/LbL substrates, as shown in the white dotted areas and boxes in Figure 4b. Our previous results suggest that the CAMA-1 cells were not seriously affected by the existence of fibronectin proteins on a substrate for their proliferation and spreading.[43] Similarly, the change in cellular shape is almost identical for the AuNP/LbL and Fn-AuNP/LbL surfaces, indicating that the adhesion of metastatic cells is mainly governed by the AuNP-based nanofeature on the surface, and the role of Fn is not so significant for the adhesion and proliferation of CAMA-1 cells.

Typically, cell adhesion is initiated by the ECM proteins. As mentioned earlier, focal adhesion kinase can affect the cytoskeleton, membrane protrusions, and cell adhesion. In the cell adhesion process, FAK also mediates phosphorylation on a specific serine residue of paxillin that binds to proteins that contribute to the organization of actin cytoskeletons, which, in turn, promotes focal adhesion remodeling and cell motility.[63,64] Thus, we performed paxillin sandwich ELISA (Figure 5a) and stained the cell with antipaxillin antibody for observing fluorescent signals using a total internal reflection fluorescence (TIRF) microscope (Figure 5b) to identify the correlation between focal adhesion and change in paxillin amount in our system. In the paxillin quantitative experiment as shown in Figure 5a, the highest values of paxillin amount were found from both AuNP/LbL and Fn-AuNP/LbL substrates. TIRF images in Figure 5b allow monitoring the interfaces between cells and a surface with high resolution and in great details. Rigorous formation of paxillin clusters was found for the cells placed on AuNP/LbL and Fn-AuNP/LbL substrates, while no distinct paxillin cluster formation was observed for the cells on other substrates. Paxillins were heavily clustered in the lamellipodium and filopodium regions, and this demonstrates that nanoparticle-featured surfaces induce pronounced paxillin clustering as well as intimate cell adhesion to the surface. Figure 5a and b show that the cells recognize nanoscale roughness by interacting with AuNPs bound to the polymer surfaces. Moreover, we took fluorescence images of phosphopaxillin (p-paxillin), which is an important element in the focal adhesion cascade signaling of cells (Figure 5c), and detected the amount p-paxillin using the Western blot method (Figure 5d). We also detected β-actin as a control protein in the Western blot experiment. The p-paxillin bands were darker and thicker for the cells on AuNP/LbL and AuNP-Fn/LbL substrates when compared with other substrates. The results again agree well with the fluorescence image results for p-paxillin. In our data, AuNP/LbL and Fn-AuNP/LbL substrates induced increased paxillin expression as well as phospohrylation of paxillins. In other words, AuNPs could activate the integrin function of metastatic cancer cells. The integrin activation stimulates the FAK signaling process, which could, in turn, result in more pronounced cellular focal adhesion. Next, we quantified the amount of integrin in CAMA-1 cells after 7 days of cell culture in order to confirm the integrin expression on the AuNP-functionalized LbL platforms through sandwich ELISA and the immunofluorescence assay (data not shown). Since metastatic cancer cells usually express notably a fewer number of integrins on their surfaces compared to normal or nonmetastatic cancer cells,[55] the change in the amount of integrin between samples was too small to be detected using conventional methods. This result indicates that AuNP/LbL and Fn-AuNP/LbL substrates stimulate the focal adhesion-associated signal pathway, while these substrates would not affect the integrin expression to a

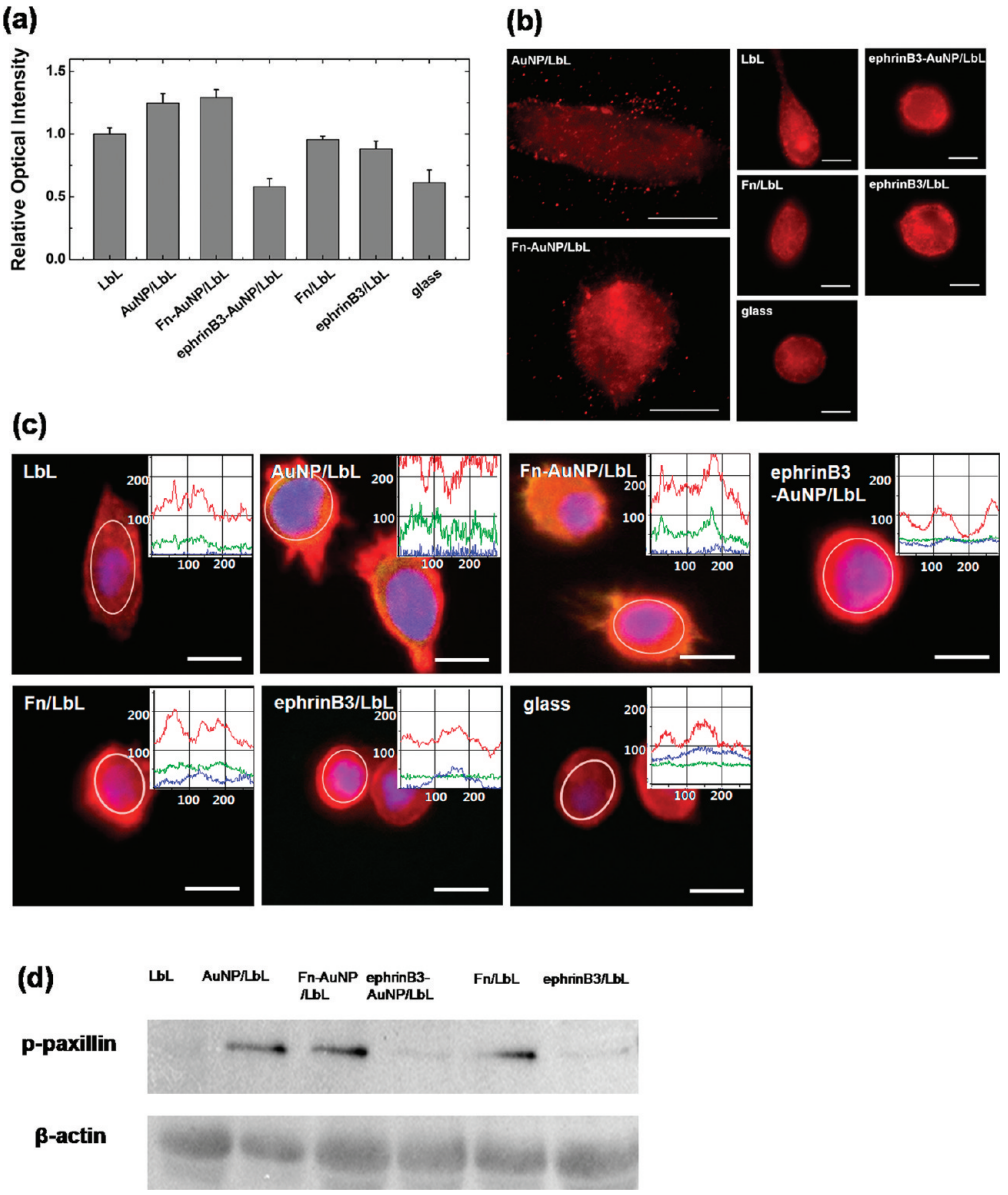

Figure 5. Paxillin analysis and imaging for CAMA-1 cells. (a) Relative paxillin amounts in CAMA-1 cells obtained by the ELISA analysis. (b) Total internal reflection fluorescence (TIRF) images of paxillins from CAMA-1 cells. The scale bars in all the images are 20 μm. (c) Fluorescence images and intensity profiles of actin (red), phospho-paxillin (green), and nucleus (blue) of the CAMA-1 cells after a 2-day culture on various substrates. The fluorescence intensity of CAMA-1 cells was obtained by circle line profiling (Image Pro Plus). We analyzed fluorescence images that had the same exposure time in the same distance intensity. (*x* axis: distance (pixels); *y* axis: fluorescence intensity) The highest values of red (actin) and green (phospho-paxillin) signals were observed from AuNP/LbL and Fn-AuNP/LbL. The scale bars in all the images are 20 μm. (d) Western blotting data for the detection of phospho-paxillin in CAMA-1 cells after a 2-day culture on various substrates. β-Actin was used as a control protein.

large extent. Notice that the focal adhesion plays a key role in the regulation of proliferation, migration, and metastasis of cancer cells.[65−67] The amount of paxillin, interacting with FAK, is closely correlated with cell proliferation,[68] and it is believed that nanofeatured substrates are more suitable for the proliferation of metastatic cells than substrates without NPs. This result suggests that the nanoscale surface topology is much more important for the adhesion and proliferation of metastatic cells than the presence of cell adhesion proteins such as fibronectin on the polymer substrate.

It has been well-known that ephrin facilitates the signaling for the detachment of metastatic cells from the surface. The roles of ephrin in reverse signaling of cancer cells have been well documented to promote cell transformation and cancer cell migration/invasion.[69,70] Two cases were examined in the present study: Ephrin molecules were directly applied on the LbL substrate (ephrinB3/LbL), and ephrinB3-conjugated AuNPs were modified to the LbL surface (ephrinB3-AuNP/LbL). For both cases, the metastatic cancer cells did not adhere to the surface effectively, and they show a round-shaped

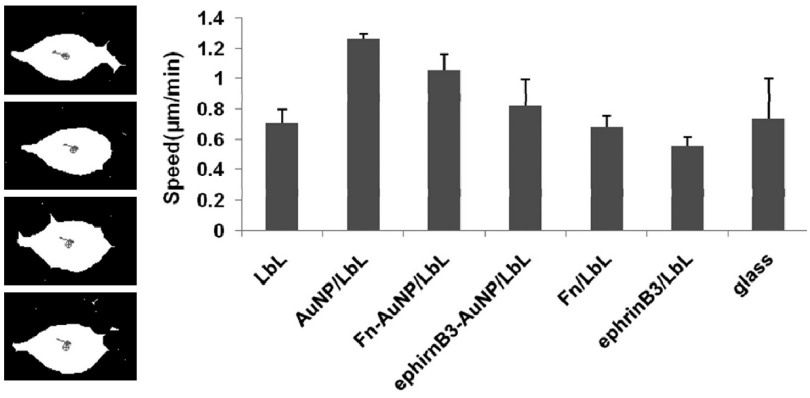

Figure 6. Change in cell speed on various substrates. After cell culturing for 2 days, the average speed of metastatic breast cancer cells (CAMA-1) was calculated from time-lapsed images by the Image Pro Plus program (four cells were sampled for each substrate). The left images are the representative center-of-cell-mass tracking images.

morphology, as shown in Figures 4 and 5. These results are comparable to the control substrates without nanoscale surface feature (*i.e.*, glass, Fn/LbL, and ephrinB3/LbL). Importantly, the amount of paxillin was distinctively lower on the ephrinB3-AuNP/LbL surface than on the ephrinB3/LbL surface (Figure 5a). All these results indicate that the ephrin signaling for focal adhesion is more effective when ephrin molecules are present on the nanostructured surface. On the other hand, the amount of detected paxillin is similar for both Fn/LbL and ephrinB3/LbL substrates. The p-paxillin fluorescence images of the cells placed on the ephrinB3-AuNP/LbL substrate also indicate that the cytoskeletal actins are mainly distributed around the edge area of a cell, and the amount of p-paxillin in the Western blot data was lower than the value on AuNP/LbL and Fn-AuNP/LbL (Figure 5c and d). This attests that focal adhesion of CAMA-1 cells was stronger for ephrin-free AuNP surfaces than other substrates. Paxillin is the first component to appear visibly organized in protrusive regions of the cells.[72] The paxillin seemed to remodel from older to new adhesion at the leading edge when a new protrusion formed. In our study, CAMA-1 cells have a polarized shape and extend protrusions with lamellipodia and filopodia on the AuNP/LbL and Fn-AuNP/LbL substrates. It is for this reason that the amounts of paxillin and p-paxillin on AuNP/LbL and Fn-AuNP/LbL are high and more paxillin clusters than on other substrates were observed in cellular protrusion areas on these nanoparticle-modified substrates (Figure 5).

The cell migration is closely related to the cell adhesion. Thus, to analyze the change in cell motility, we obtained the cell speed estimated from time-lapsed cell images using the Image Pro Plus program (Figure 6; four cells were sampled for each substrate). The traveled distance by a cell was measured by comparing the cell centers of mass in two consecutive image frames. The measured distance was then divided by the time interval to calculate the cell speed. The overall trend reveals that nanoparticle-modified surfaces generate higher cell speed; any kind of AuNP modification on the LbL surfaces yields more positive change in the cell speed when compared with simple Fn or ephrin modifications on the LbL surfaces (Figure 6; compare the cell speeds for LbL *vs* AuNP/LbL, Fn-AuNP/LbL *vs* Fn/LbL, and ephrin-AuNP/LbL *vs* ephrin/LbL, respectively). These results also suggest that ephrin modification not only changes the cell shape to spherical but also lowers the cell speed when compared with equivalent Fn modification. The highest cell speed value was obtained with AuNP/LbL substrate, featuring large cell spreading with filopodia and lamellipodia, strong actin bundle formation, and focal adhesion (Figures 4–6). It is well-known that cancer cell motility is involved with integrin signaling, focal-contact formation, and actomyosin-dependent contractility. For effective cell migration, the cell body must modify its shape and stiffness to interact with surrounding tissue structure.[71,72] Our results for human breast metastatic cancer cells are in good agreement with other observations for breast cancer and ovarian cancer cells. The data in the present study showed that the focal adhesion as well as the invasiveness of metastatic cancer cells is closely correlated with the migration of tumor cells.

CONCLUSION

In this study, Au nanoparticle-modified LbL polymer substrate offers a nanotopological, biologically functional, and flexible platform for understanding and controlling the phenotypic changes of human breast metastatic cancer cells. An LbL polymer film provides a handle to control surface charge and mechanical properties that allow for mimicking an *in vivo*-like extracellular matrix. Further, this platform also offers a versatile and flexible substratum to easily modify nanoparticles and to create intimate contacts between cells and the surface. Our results suggest that the AuNP surface density and nanoclustered proteins on a spherical AuNP are critical factors for the efficient signaling and interfacing of metastatic cells. The existence of nanotopological features (AuNPs in this case) is much more important than the presence of Fn, a cell adhesion protein, in inducing more

dramatic changes in metastatic cell adhesion, protrusion, polarity, and motility. Importantly, metastatic cell adhesion is largely affected by AuNP surface density, and relatively large spacing (~1.7 μm) between AuNPs is optimal for metastatic cell adhesion to the AuNP/LbL surface. We further found that AuNP-modified LbL surfaces caused effective cell adhesion through the stimulation of phosphorylation of paxillin by tyrosine kinase with rigorous cell surface projections that is similar to Fn-AuNP-modified LbL surfaces, indicating high cell motility, even in the absence of Fn on the surface. Moreover, the ephrin signaling for reduced focal adhesion and cell detachment was found to be more effective when the ephrinB3 was exposed to metastatic cells in an ephrinB3-modified AuNP form, while the negative focal adhesion signaling was not effective when ephrin was directly attached to the LbL surface. The results imply that nanotopology and three-dimensional protein clusters are critical in controlling and understanding phenotypic changes and intracellular signaling of metastatic cancer cells and their invasion mechanism. We believe that the strategies and results shown in this study are important in constructing more natural metastatic cell-interfacing platforms and in studying and controlling metastatic cancer cells, and eventually could give insights for metastatic cancer research, diagnosis, and treatment.

METHODS

Materials. Poly(allylamine hydrochloride) (M_w = 70 000 g/mol) and poly(acrylic acid) (M_w = 100 000 g/mol) were purchased from Aldrich. Fibronectin from human plasma (Fn, M_w = 450 000 g/mol) and ephrinB3 (M_w = 49 200 g/mol) were purchased from Sigma and used as received. Cryo-preserved human breast cancer cell line and media were purchased from American Type Culture Collection (Manassas, VA, USA).

Preparation of Layer-by-Layer Polymer Films. PAA and PAH polymer solutions (0.01 M) were prepared by dissolving the polymers in 18 MΩ Mili-Q water, and HCl and NaOH were used for the pH adjustment, at pH 7.5 for PAH and at pH 3.5 for PAA. Fibronectin and ephrinB3 were also dissolved in water (0.67 mg/mL) prior to use. Cover glass was used as a substrate to build the LbL film. All the substrates were cleaned by RCA treatments[73] before LbL deposition. $(PAH/PAA)_5$/PAH LbL polymer films were prepared using an automatic spin coater (Headway Research Inc.). Detailed experimental descriptions for the LbL deposition process are well-documented in our previous report.[20] For the modification of an LbL film with nanoparticles, AuNP and protein-modified AuNPs (Fn-AuNP and ephrinB3-AuNP, respectively) in water were added to the PAH top-coated LbL film and spun at 3000 rpm for 20 s until a sufficiently dried film was obtained. The coated AuNP density was controlled by varying the spin-coating time and concentration of gold particle solution (4.5×10^{10}/mL).

Characterization of LbL Films. The film surface morphology and rms roughness were measured by an AFM microscope (Nanoscope IIIa, Digital Instruments). Water contact angles were measured using a DE/DSA100 (Früss Inc.) contact angle analyzer.

Au Nanoparticle Probe Preparation. First, the pH of a gold nanoparticle solution (Ted Pella, USA, 15708-55) was increased to pH 9 by NaOH solution to obtain a sufficient interaction between the gold nanoparticles and proteins. Then, fibronectin or ephrinb3 proteins were added to 1 mL of gold nanoparticle solution (concentration 0.7 mg/mL). The amount of protein was determined by a salt test to see whether Au nanoparticles are aggregated or dispersed when the final salt concentration of the solution reaches 0.2 M. After 1 h incubation, gold nanoparticles were precipitated by centrifugation at 8000 rpm, 4 °C. The supernatant was removed, and then the gold nanoparticles were dispersed in distilled water.

Bradford Assay for the Quantification of Coated Proteins on AuNPs. We performed the Bradford assay (Bio-Rad, USA, 500-0006) to calculate the amount of coated protein per AuNP. A 50 nm AuNP solution (1 mL, AuNP solution pH = 9) was incubated with either fibronectin or ephrinB3 (20 μL, the protein stock solution concentration was 0.7 mg/mL) in a tube for 1 h. The AuNPs were precipitated by centrifugation at 8500 rpm, 4 °C for 15 min, and the supernatant was removed to measure the amount of unreacted proteins in solution. We measured the amount of proteins in the supernatant using the Bradford assay. This method is based on the observation that the absorbance maximum of an acidic solution of Coomassie Brilliant Blue G-250 changes from 465 to 595 nm when it binds to proteins. Both hydrophobic and ionic interactions stabilize the anionic form of the dye, causing a visible color change. The sample solution diluted with distilled water (160 μL) was added into a microliter plate well. Then we added 40 μL of dye reagent concentrate to each well and mixed the sample with reagent thoroughly using a multichannel pipet to dispense the reagent. After 5 min, we obtained the standard curve and remaining-protein data at 595 nm using a plate reader (BioTek, USA, ELx-800). Finally, we calculated the amount of coated protein per AuNP (the amount of initially added proteins − remaining protein amount = coated proteins). In the case of 2 μg Fn (440 kDa) modification to AuNP solution (4.5×10^{10} AuNPs/mL), we found that ~60 protein molecules were modified to a single AuNP, which may cover a ~9225 nm^2 surface area. For 5 μg of ephrinB3 protein (36 kDa), ~180 protein molecules were modified to a single AuNP. These proteins could cover a ~7480 nm^2 surface area. A single 50 nm AuNP has a surface area of 7850 nm^2. Therefore, it is likely that an ephrinB3 protein monolayer is covering the AuNPs surface, while Fn covers the AuNP surface with more than a monolayer. The dynamic light scattering data further support that Fn forms multiple layers on the AuNP surface (Supporting Table S1).

Zeta Potential and DLS Measurements. The surface zeta potential and hydrodynamic diameters of the Au nanoparticles were measured by a dynamic light scattering spectrophotometer (Ohtsuka Electronics, Japan, DLS-7000). Three kinds of Au nanoparticles (citrate-stabilized AuNP, fibronectin-modified AuNP, and ephrinB3-modified AuNP) were centrifuged and redispersed in pure water, respectively. Zeta potential and hydrodynamic diameter values were evaluated three times for each case.

Cell Culture. The CAMA-1 cells (ATCC No. HTB-21) were purchased from ATCC. CAMA-1 cells (cell concentration 1×10^4 cells) were grown in DMEM (ATCC) with 10% fetal bovine serum and 100 units/mL penicillin−streptomycin (Gibco, USA, 15070063) at 37 °C, 5% CO_2. For more exclusive observation of substrate effect, CAMA-1 cells were cultured in DMEM media without FBS for 2 or 7 days at 37 °C, 5% CO_2.

Analysis of Cell Aspect Ratio. The CAMA-1 cells were cultured for 2 days. Then, we took the optical images of cells using optical microscopy (10×; Carl Zeiss, Germany, Axiovert 200M). We calculated the aspect ratio of 60 cells present in the optical images of each sample. To calculate the aspect ratio, two different principal lengths of the cells were measured: the longest and shortest line lengths. The longest line length is literally the longest line length of the cell body, and the shortest line length is taken at the direction orthogonal to the longest line length. Dividing the longest line length by the shortest one defines the aspect ratio.

Actin Staining. The cell culture medium was harvested, and cells were washed twice with PBS solution. Cells were then fixed by 4% paraformaldehyde/PBS for 15 min. Cells were washed with PBS solution three times (5 min each time). To block nonspecific binding,

we used 1% BSA/PBS/0.3% Tween20 for 15 min, and the cells were washed with PBS solution afterward. Phalloidin/tetramethylrhodamine isothiocyanate (TRITC) (Sigma-Aldrich, USA, P-1951) was diluted to 5% with PBS solution. The phalloidin/TRITC solution was added to each well, and the cells were incubated at 37 °C for 40 min. Next, cells were washed with PBS solution two times after incubation. Finally, the stained cell samples were examined under a confocal laser scanning microscope (Leica, Germany, TCS SP5).

Sandwich ELISA. The amount of focal adhesion-associated protein, paxillin, in cell extracts was evaluated with the sandwich ELISA method. CAMA-1 cells were grown in DMEM with 10% fetal bovine serum and 100 units/mL penicillin−streptomycin (Gibco, USA, 15070063) for 2 days. Cells were disrupted by RIPA buffer (Pierce, USA, 89900) at 4 °C. Lysates were clarified at 14 000 rpm in an Eppendorf tube for 10 min at 4 °C. The supernatant was transferred to a new tube, and the pellet was discarded. We performed the Bradford assay (Bio-Rad, USA, 500-0006) to determine the protein concentration. For the sandwich assay, samples were loaded on 96 wells. We used rabbit anti-human paxillin polyclonal antibody (abcam, United Kingdom, ab2264) and mouse anti-human paxillin monoclonal antibody (abcam, United Kingdom, ab3127) to form sandwich complexes. At the final step, secondary anti-rabbit IgG was conjugated to horseradish peroxidase, and the absorbance at 450 nm was measured.

Transmission Electron Microscopy Specimen Preparation for Sectioned Cell Samples. Cells were detached from the substrate by trypsin-EDTA. Centrifugation was carried out to move the cells to the tube bottom. The cells were primarily fixed (at 4 °C for 4 h) with modified Karnovsky fixative (2% paraformaldehyde and 2% glutaraldehyde in 0.05 M sodium cacodylate buffer pH 7.2). Then, the specimen was washed using 0.05 M sodium cacodylate buffer (pH 7.2). In post-fixation, 1% osmium tetroxide in 0.05 M sodium cacodylate buffer (pH 7.2) was used and incubated for 2 h. After washing with distilled water, we treated with 0.5% uranyl acetate for En bloc staining. The next step in the preparation process was dehydration with 30% to 100% ethanol for 10 min each. After transition and infiltration, the sample was molded with Spurr's resin at 70 °C for 24 h and sectioned for TEM measurement. The sectioned specimen was stained with 2% uranyl acetate and Reynold's lead citrate. We observed the samples using a TEM (LIBRA 120, Carl Zeiss, Germany).

Paxillin and Phospho-paxillin Staining. After cell culturing for 2 days, cells were fixed in 3.7% paraformaldehyde in PBS solution at pH 7.4 for 20 min at room temperature. Then, the samples were washed twice with cold PBS solution. The samples were incubated with PBS solution containing 0.25% Triton X-100 for 10 min. Next, cells were washed with PBS solution three times for 5 min each. These samples were treated with 1% BSA in PBST for 30 min to block nonspecific binding of the antibodies. Cells were then incubated in the anti-paxillin antibody (abcam, United Kingdom, ab3127) or anti-phospho-paxillin antiboby (Ser126) (Millipore, USA, 07-733SP) solution with blocking buffer overnight at 4 °C. On the following day, cells were washed three times with PBS solution for 5 min each. For paxillin staining, cells were incubated with rhodamine-conjugated secondary antibody (abcam, United Kigndom) in 1% BSA for 1 h at room temperature without exposing to light. In the anti-phopho-paxillin staining case, cells were incubated with FITC-conjugated secondary antibody (Millipore, USA). We decanted the secondary antibody solution and washed three times with PBS solution for 5 min each in the dark. Finally, we mounted a drop of mounting medium (abcam, United Kingdom, ab64230) on a coverslip. Paxiilin was observed by a total internal reflection fluorescence microscope (60×; Nikon, Japan, TE2000-E) with the same exposure time. We took phospho-paxillin images using florescence microscopy (40×; Carl Zeiss, Germany, Axiovert 200M).

Western Blot. We performed Western blotting to compare the protein amount of cells for each substrate. First, CAMA-1 cells were cultured in DMEM with 10% FBS on LbL, Fn/LbL, ephrinB3/LbL, AuNPs/LbL, Fn-AuNPs/LbL, and ephrinB3-AuNPs/LbL substrates, respectively, at 37 °C, 5% CO_2 for 2 days. Then, the cells were collected and transferred to microcentrifuge tubes. To remove cell culture medium, the tubes were centrifuged at 1500 rpm for 3 min. For cell lysis, we added RIPA buffer (Pierce, USA, 89900) to each tube, and a total protein solution was obtained. We diluted an aliquot of the cell lysate sample for the Bradford (Bio-Rad, USA, 500-0006) protein concentration assay. Next, we added an equal volume of 2× sample buffer (125 mM Tris pH 6.8, 4% SDS, 10% glycerol, 0.006% bromophenol blue, and 1.8% ss-mercaptoethanol) to all samples, and the resulting solution was boiled for 3−5 min. A 10 μg amount of total proteins of cells was added to each well of a 10% SDS 0.75 mm thick gel (Hoefer, Germany). The proteins were transferred from the gel to a PVDF membrane at 1 amp constant current for 1 h or equivalent in transfer buffer (Hoefer, Germany). The blot from the transfer apparatus was removed and immediately placed into blocking buffer (5% nonfat dry milk, 10 mM Tris pH 7.5, 100 mM NaCl, and 0.1% Tween 20). The membrane was incubated in blocking buffer for 1 h at room temperature. We diluted the antibody according to the antibody data sheet in the corresponding blocking buffer [β-actin antibody (rabbit, Santa Cruz, USA) 1:5000, p-paxillin antibody (rabbit, Millipore, USA) 1:500]. After decanting the blocking buffer from the blot, we added the antibody solution, and the resulting solution was incubated with agitation overnight at 4 °C. After decanting the primary antibody solution, the membrane was washed with wash buffer (10 mM Tris pH 7.5, 100 mM NaCl, and 0.1% Tween 20) for 30 min with agitation, changing the wash buffer every 3−5 min. We added diluted-enzyme conjugate anti-rabbit IgG-HRP (1:5000 in wash buffer containing 5% nonfat dry milk), and the resulting solution was incubated with agitation for 1 h at room temperature. We decanted the secondary antibody solution and added wash buffer (10 mM Tris pH 7.5, 100 mM NaCl, 0.1% Tween 20), and the membrane was washed for 1.5 h with agitation, changing the wash buffer every 20 min. Finally, we added ECL mix (GE Healthcare, U.K.) to the membrane, and the signal of the membrane was immediately exposed to film for 1 min.

Time-Lapsed Live-Cell Imaging. We imaged CAMA-1 cell behavior on a prepared polymer platform immediately after or 48 h after seeding cells to substrates by time-lapsed microscopy. Cells were in a Chamlide incubation system, which maintains 37 °C and 5% CO_2 conditions, for the microscopy (Live Cell Instrument, Cu-104). Live-cell images were taken at 1 min intervals over 2 h using 60× or 20× objective lenses (Nikon, Japan, TE2000-E).

Cell Speed Analysis. We used the Image Pro Plus program (ver. 6.3) to make a comparison between CAMA-1 cells, which were cultured for 48 h, for their motility on prepared platforms. This program tracked cells' center of mass in images that were taken by a 20× objective lens (above description). Before tracking the cells, we made sequence files of time-lapsed cell images. The images of each sequence were changed to gray scale, and the background signal was removed using the program's filter system. Then we designated the cell to measure migration length. Finally, the velocity of the cells on the substrate was calculated. We repeated the same procedure four times.

Nonspecific Binding Test. We confirmed nonspecific interaction between fibronectin and polymer substrates. The samples were incubated in DMEM with 10% NCS (newborn calf serum, Gibco, USA) for 48 h. Then these substrates were washed twice with PBS for 3 min each and incubated with anti-fibronectin antibody (Millipore, USA) solution overnight at 4 °C. We used rhodamine-conjugated secondary antibody (abcam, United Kingdom) to detect fibronectin. The images were observed by florescence microscopy (Carl Zeiss, Germany, Axiovert 200M).

Acknowledgment. This work was supported by the National Research Foundation of Korea (NRF) grant funded by the Korean government (MEST) (No. 2011-0018198), the 21C Frontier Functional Proteomics Project (No. 2011K00135) through the National Research Foundation of Korea (NRF) from the Ministry of Education, Science and Technology, and the Industrial Core Technology Development Program of the Ministry of Knowledge Economy (No. 10033467-2010-12). This work was additionally supported by the National Creative Research Initiative Center for Intelligent Hybrids (No. 2010-0018290) through the National Research Foundation of Korea (NRF) grants, the World Class University (WCU) Programs (R31-10013), and the Brain Korea 21 Program funded by the Ministry of Education, Science and Technology (MEST). H.L., Y.J., and J.S. are also grateful for the financial support from the Seoul Science Fellowship.

Supporting Information Available: Hydrodynamic diameter of AuNP, Fn-AuNP, and ephrinB3-AuNP (Table S1). Experimental conditions for controlling AuNP densities (Table S2). Fibronectin

immunostaining data (Figure S1). Optical images of CAMA-1 cells in DMEM with 10% NCS (Figure S2). Optical images of CAMA-1 cells in DMEM without FBS (Figure S3). Time-lapsed images of CAMA-1 cells (Figure S4). Optical images of CAMA-1 cells after 7 days of culture (Figure S5). This material is available free of charge *via* the Internet at http://pubs.acs.org.

REFERENCES AND NOTES

1. Gupta, G. P.; Massagu, J. Cancer Metastasis: Building a Framework. *Cell* **2006**, *127*, 679–695.
2. Akiyama, S. K.; Olden, K.; Yamada, K. M. Fibronectin and Integrins in Invasion and Metastasis. *Cancer Metastasis Rev.* **1995**, *14*, 173–189.
3. Tanaka, M.; Sackmann, E. Polymer-Supported Membranes as Models of the Cell Surface. *Nature* **2005**, *437*, 656–663.
4. Liu, W. F.; Chen, C. S. Engineering Biomaterials to Control Cell Function. *Mater. Today* **2005**, *8*, 28–35.
5. Doh, J.; Irvine, D. J. Immunological Synapse Arrays: Patterned Protein Surfaces that Modulate Immunological Synapse Structure Formation in T cells. *Proc. Natl. Acad. Sci. U. S. A* **2006**, *103*, 5700–5705.
6. Torres, A. J.; Wu, M.; Holowka, D.; Baird, B. Nanobiotechnology and Cell Biology: Micro- and Nanofabricated Surfaces to Investigate Receptor-Mediated Signaling. *Annu. Rev. Biophys.* **2008**, *37*, 265–288.
7. Tang, Z. Y.; Wang, Y.; Podsiadlo, P.; Kotov, N. A. Biomedical Applications of Layer-by-Layer Assembly: From Biomimetics to Tissue Engineering. *Adv. Mater.* **2006**, *18*, 3203–3224.
8. Boudou, T.; Crouzier, T.; Ren, K. F.; Blin, G.; Picart, C. Multiple Functionalities of Polyelectrolyte Multilayer Films: New Biomedical Applications. *Adv. Mater.* **2010**, *22*, 441–467.
9. Mendelsohn, J. D.; Yang, S. Y.; Hiller, J.; Hochbaum, A. I.; Rubner, M. F. Rational Design of Cytophilic and Cytophobic Polyelectrolyte Multilayer Thin Films. *Biomacromolecules* **2003**, *4*, 96–106.
10. Zheng, H.; Berg, M. C.; Rubner, M. F.; Hammond, P. T. Controlling Cell Attachment Selectively onto Biological Polymer-Colloid Templates Using Polymer-on-Polymer Stamping. *Langmuir* **2004**, *20*, 7215–7222.
11. Wittmer, C. R.; Phelps, J. A.; Saltzman, W. M.; Van Tassel, P. R. Fibronectin Terminated Multilayer Films: Protein Adsorption and Cell Attachment Studies. *Biomaterials* **2007**, *28*, 851–860.
12. Ren, K.; Crouzier, T.; Roy, C.; Picart, C. Polyelectrolyte Multilayer Films of Controlled Stiffness Modulate Myoblast Cell Differentiation. *Adv. Funct. Mater.* **2008**, *18*, 1378–1389.
13. Khademhosseini, A.; Suh, K. Y.; Yang, J. M.; Eng, G.; Yeh, J.; Levenberg, S.; Langer, R. Layer-by-Layer Deposition of Hyaluronic Acid and Poly-Lysine for Patterned Cell Co-cultures. *Biomaterials* **2004**, *25*, 3583–3592.
14. Salloum, D. S.; Olenych, S. G.; Keller, T. C. S.; Schlenoff, J. B. Vascular Smooth Muscle Cells on Polyelectrolyte Multilayers: Hydrophobicity-Directed Adhesion and Growth. *Biomacromolecules* **2005**, *6*, 161–167.
15. Thompson, M. T.; Berg, M. C.; Tobias, I. S.; Rubner, M. F.; Van Vliet, K. J. Tuning Compliance of Nanoscale Polyelectrolyte Multilayers to Modulate Cell Adhesion. *Biomaterials* **2005**, *26*, 6836–6845.
16. Schneider, A.; Francius, G.; Obeid, R.; Schwinte, P.; Hemmerle, J.; Frisch, B.; Schaaf, P.; Voegel, J. C.; Senger, B.; Picart, C. Polyelectrolyte Multilayers with a Tunable Young's Modulus: Influence of Film Stiffness on Cell Adhesion. *Langmuir* **2006**, *22*, 1193–1200.
17. Picart, C.; E., R.; Richert, L.; Audoin, F.; Arntz, Y.; Cardoso, M. D. S.; Schaaf, P.; Voegel, J. C.; Frisch, B. Primary Cell Adhesion on RGD-Functionalized and Covalently Crosslinked Thin Polyelectrolyte Multilayer Films. *Adv. Funct. Mater.* **2005**, *15*, 83–94.
18. Thompson, M. T.; Berg, M. C.; Tobias, I. S.; Lichter, J. A.; Rubner, M. F.; VanVliet, K. J. Biochemical Functionalization of Polymeric Cell Substrata Can Alter Mechanical Compliance. *Biomacromolecules* **2006**, *7*, 1990–1995.
19. Stevens, M. M.; George, J. H. Exploring and Engineering the Cell Surface Interface. *Science* **2005**, *310*, 1135–1138.
20. Du, D.; Liu, S.; Chen, J.; Ju, H.; Lian, H.; Li, J. Colloidal Gold Nanoparticle Modified Carbon Paste Interface for Studies of Tumor Cell Adhesion and Viability. *Biomaterials* **2005**, *26*, 6487–6495.
21. Bettinger, C.; Langer, R.; Borenstein, J. Engineering Substrate Topography at the Micro- and Nanoscale to Control Cell Function. *Angew. Chem., Int. Ed.* **2009**, *48*, 5406–5415.
22. Lim, J. Y.; Donahue, H. J. Cell Sensing and Response to Micro- and Nanostructured Surfaces Produced by Chemical and Topographic Patterning. *Tissue Eng.* **2007**, *13*, 1879–1891.
23. Torres, A. J.; Wu, M.; Holowka, D.; Baird, B. Nanobiotechnology and Cell Biology: Micro- and Nanofabricated Surfaces to Investigate Receptor-Mediated Signaling. *Annu. Rev. Biophys.* **2008**, *37*, 265–288.
24. Sniadecki, N.; Desai, R.; Ruiz, S.; Chen, C. Nanotechnology for Cell−Substrate Interactions. *Ann. Biomed. Eng.* **2006**, *34*, 59–74.
25. Mossman, K. D.; Campi, G.; Groves, J. T.; Dustin, M. L.; Altered, T. C. R. Signaling from Geometrically Repatterned Immunological Synapses. *Science* **2005**, *310*, 1191–1193.
26. Sekula, S.; Fuchs, J.; Weg-Remers, S.; Nagel, P.; Schuppler, S.; Fragala, J.; Theilacker, N.; Franzreb, M.; Wingren, C.; Lenhert, S.; *et al*. Multiplexed Lipid Dip-Pen Nanolithography on Subcellular Scales for the Templating of Functional Proteins and Cell Culture. *Small* **2008**, *4*, 1785–1793.
27. Yim, E. K. F.; Darling, E. M.; Kulangara, K.; Guilak, F.; Leong, K. W. Nanotopography-Induced Changes in Focal Adhesions, Cytoskeletal Organization, and Mechanical Properties of Human Mesenchymal Stem Cells. *Biomaterials* **2010**, *31*, 1299–1306.
28. Yang, L.; Sheldon, B. W.; Webster, T. J. The Impact of Diamond Nanocrystallinity on Osteoblast Functions. *Biomaterials* **2009**, *30*, 3458–3465.
29. Doh, J.; Irvine, D. J. Immunological Synapse Arrays: Patterned Protein Surfaces that Modulate Immunological Synapse Structure Formation in T Cells. *Proc. Natl. Acad. Sci. U. S. A* **2006**, *103*, 5700–5705.
30. Salaita, K.; Nair, P. M.; Petit, R. S.; Neve, R. M.; Das, D.; Gray, J. W.; Groves, J. T. Restriction of Receptor Movement Alters Cellular Response: Physical Force Sensing by EphA2. *Science* **2010**, *327*, 1380–1385.
31. Park, J.; Bauer, S.; von der Mark, K.; Schmuki, P. Nanosize and Vitality: TiO_2 Nanotube Diameter Directs Cell Fate. *Nano Lett.* **2007**, *7*, 1686–1691.
32. Murphy, C. J.; Gole, A. M.; Stone, J. W.; Sisco, P. N.; Alkilany, A. M.; Goldsmith, E. C.; Baxter, S. C. Gold Nanoparticles in Biology: Beyond Toxicity to Cellular Imaging. *Acc. Chem. Res.* **2008**, *41*, 1721.
33. Ranzinger, J.; Krippner-Heidenreich, A.; Haraszti, T.; Bock, E.; Tepperink, J.; Spatz, J. P.; Scheurich, P. Nanoscale Arrangement of Apoptotic Ligands Reveals a Demand for a Minimal Lateral Distance for Efficient Death Receptor Activation. *Nano Lett.* **2009**, *9*, 4240.
34. Wang, S.; Wang, H.; Jiao, J.; Chen, K.-J.; Owens, G. E.; Kamei, K.-i.; Sun, J.; Sherman, D. J.; Behrenbruch, C. P.; Tseng, H.-R.; *et al*. Three-Dimensional Nanostructured Substrates toward Efficient Capture of Circulating Tumor Cells. *Angew. Chem.* **2009**, *121*, 9132.
35. Huang, J.; Ding, J. Nanostructured Interfaces with RGD Arrays to Control Cell-Matrix Interaction. *Soft Matter* **2010**, *6*, 3395.
36. Bartczak, D.; Muskens, O. L.; Millar, T. M.; Sanchez-Elsner, T.; Kanaras, A. G. Laser-Induced Damage and Recovery of Plasmonically Targeted Human Endothelial Cells. *Nano Lett.* **2011**, *11*, 1358.
37. Farokhzad, O. C.; Langer, R. Impact of Nanotechnology on Drug Delivery. *ACS Nano* **2009**, *3*, 16.
38. Qian, X.; Peng, X.-H.; Ansari, D. O.; Yin-Goen, Q.; Chen, G. Z.; Shin, D. M.; Yang, L.; Young, A. N.; Wang, M. D.; Nie, S. *In Vivo* Tumor Targeting and Spectroscopic Detection with Surface-Enhanced Raman Nanoparticle Tags. *Nat. Biotechnol.* **2008**, *26*, 83.

39. Lackmann, M.; Boyd, A. W. Eph, a Protein Family Coming of Age: More Confusion, Insight, or Complexity. *Sci. Signal.* **2008**, *1*, re2.
40. Nakada, M.; Drake, K. L.; Nakada, S.; Niska, J. A.; Berens, M. E. Ephrin-B3 Ligand Promotes Glioma Invasion through Activation of Rac1. *Cancer Res.* **2006**, *2006*, 8492–8500.
41. Merlos-Suárez, A.; Batlle, E. Eph-ephrin Signalling in Adult Tissues and Cancer. *Curr. Opin. Cell Biol.* **2008**, *20*, 194–200.
42. Aoto, J.; Chen, L. Bidirectional ephrin/Eph Signaling in Synaptic Functions. *Brain Res.* **2007**, *1184*, 72–80.
43. Seo, J.; Lee, H.; Jeon, J.; Jang, Y.; Kim, R.; Char, K.; Nam, J.-M. Tunable Layer-by-Layer Polyelectrolyte Platforms for Comparative Cell Assays. *Biomacromolecules* **2009**, *10*, 2254–2260.
44. Sniadecki, N.; Desai, R. A.; Ruiz, S. A.; Chen, C. S. Nanotechnology for Cell-Substrate Interactions. *Ann. Biomed. Eng.* **2006**, *34*, 59–74.
45. Cho, J.; Char, K.; Hong, J. D.; Lee, K. B. Fabrication of Highly Ordered Multilayer Films Using a Spin Self-Assembly Method. *Adv. Mater.* **2001**, *13*, 1076–1078.
46. Tanaka, M.; Sackmann, E. Polymer-supported Membranes as Models of the Cell Surface. *Nature* **2005**, *437*, 656–663.
47. Owen, J. D.; Ruest, P. J.; Fry, D. W.; Hanks, S. K. Induced Focal Adhesion Kinase (FAK) Expression in FAK-Null Cells Enhances Cell Spreading and Migration Requiring Both Auto- and Activation Loop Phosphorylation Sites and Inhibits Adhesion-Dependent Tyrosine Phosphorylation of Pyk2. *Mol. Cell. Biol.* **1999**, *19*, 4806–4818.
48. Webb, D. J.; Donais, K.; Whitmore, L. A.; Thomas, S. M.; Turner, C. E.; Parsons, J. T.; Horwitz, A. F. FAK-Src Signalling through Paxillin, ERK and MLCK Regulates Adhesion Disassembly. *Nat. Cell Biol.* **2004**, *6*, 154–161.
49. Schaller, M. D.; Parsons, J. T. pp125FAK-Dependent Tyrosine Phosphorylation of Paxillin Creates a High-Affinity Binding Site for Crk. *Mol. Cell. Biol.* **1995**, *15*, 2635–2645.
50. Chen, C. S.; Mrksich, M.; Huang, S.; Whitesides, G. M.; Ingber, D. E. Geometric Control of Cell Life and Death. *Science* **1997**, *276*, 1425–1428.
51. Arnold, M.; Cavalcanti-Adam, E. A.; Glass, R.; Blümmel, J.; Eck, W.; Kantlehner, M.; Kessler, H.; Spatz, J. P. Activation of Integrin Function by Nanopatterned Adhesive Interfaces. *ChemPhysChem* **2004**, *5*, 383–388.
52. Arnold, M.; Schwieder, M.; Blummel, J.; Cavalcanti-Adam, E. A.; Lopez-Garcia, M.; Kessler, H.; Geiger, B.; Spatz, J. P. Cell Interactions with Hierarchically Structured Nano-patterned Adhesive Surfaces. *Soft Matter* **2009**, *5*, 72–77.
53. Arnold, M.; Hirschfeld-Warneken, V. C.; Lohmü ller, T.; Heil, P.; Blümmel, J.; Cavalcanti-Adam, E. A.; Ló pez-García, M. n.; Walther, P.; Kessler, H.; Geiger, B.; Spatz, J. P. Induction of Cell Polarization and Migration by a Gradient of Nanoscale Variations in Adhesive Ligand Spacing. *Nano Lett.* **2008**, *8*, 2063–2069.
54. Kunzler, T. P.; Huwiler, C.; Drobek, T.; V, J.; Spencer, N. D. Systematic Study of Osteoblast Response to Nanotopography by Means of Nanoparticle-Density Gradients. *Biomaterials* **2007**, *28*, 5000–5006.
55. Zimmerberg, J.; Kozlov, M. M. How Proteins Produce Cellular Membrane Curvature. *Nat. Rev. Mol. Cell Biol.* **2006**, *7*, 9–19.
56. Huang, J.; Gräter, S. V.; Corbellini, F.; Rinck, S.; Bock, E.; Kemkemer, R.; Kessler, H.; Ding, J.; Spatz, J. P. Impact of Order and Disorder in RGD Nanopatterns on Cell Adhesion. *Nano Lett.* **2009**, *9*, 1111–1116.
57. Abe, Y.; Tsutsui, T.; Mu, J.; Kosugi, A.; Yagita, H.; Sobue, K.; Niwa, O.; Fujiwara, H.; Hamaoka, T. A Defect in Cell-to-cell Adhesion *via* Integrin-Fibronectin Interactions in a Highly Metastatic Tumor Cell Line. *Cancer Sci.* **1997**, *88*, 64–71.
58. Sommers, C. L.; Byers, S. W.; Thompson, E. W.; Torri, J. A.; Gelmann, E. P. Differentiation State and Invasiveness of Human Breast Cancer Cell Lines. *Breast Cancer Res. Treat.* **1994**, *31*, 325–335.
59. Pan, H.; Wanami, L.; Dissanayake, T.; Bachelder, R. Autocrine Semaphorin3A Stimulates alpha2 beta1 Integrin Expression/Function in Breast Tumor Cells. *Breast Cancer Res. Treat.* **2009**, *118*, 197–205.
60. Murphy-Ullrich, J. E. The De-adhesive Activity of Matricellular Proteins: is Intermediate Cell Adhesion an Adaptive Atate. *J. Clin. Invest.* **2001**, *107*, 785–790.
61. Kaibuchi, K.; Kuroda, S.; Amano, M. Regulation of The Cytoskeleton and Cell Adhesion by the RHO Family GTPases in Mammalian Cells. *Annu. Rev. Biochem.* **1999**, *68*, 459–486.
62. Dobrzyńska, I. S.-P.; Sulkowski, B.; Figaszewski, S. Changes in Electric Charge and Phospholipids Composition in Human Colorectal Cancer Cells. *Mol. Cell. Biochem.* **2005**, *276*, 113–119.
63. Mitra, S. K.; Hanson, D. A.; Schlaepfer, D. D. Focal Adhesion Kinase: in Command and Control of Cell Motility. *Nat. Rev. Mol. Cell Biol.* **2005**, *6*, 56–68.
64. McLean, G. W.; Carragher, N. O.; Avizienyte, E.; Evans, J.; Brunton, V. G.; Frame, M. C. The Role of Focal-Adhesion Kinase in Cancer—a New Therapeutic Opportunity. *Nat. Rev. Cancer* **2005**, *5*, 505–515.
65. Geiger, B.; Spatz, J. P.; Bershadsky, A. D. Environmental Sensing through Focal Adhesions. *Nat. Rev. Mol. Cell Biol.* **2009**, *10*, 21–33.
66. Melkoumian, Z. K.; Peng, X.; Gan, B.; Wu, X.; Guan, J.-L. Mechanism of Cell Cycle Regulation by FIP200 in Human Breast Cancer Cells. *Cancer Res.* **2005**, *65*, 6676–6684.
67. Wang, D.; Grammer, J.; Cobbs, C.; Stewart, J.; Liu, Z.; Rhoden, R.; Hecker, T.; Ding, Q.; Gladson, C. p125 Focal Adhesion Kinase Promotes Malignant Astrocytoma Cell Proliferation *in Vivo*. *J. Cell Sci.* **2000**, *113*, 4221–4230.
68. Cox, B. D.; Natarajan, M.; Stettner, M. R.; Gladson, C. L. New Concepts Regarding Focal Adhesion Kinase Promotion of Cell Migration and Proliferation. *J. Cell Biochem.* **2006**, *99*, 35–52.
69. Campbell, T. N.; Attwell, S.; Arcellana-Panlilio, M.; Robbins, S. M. Ephrin A5 Expression Promotes Invasion and Transformation of Murine Fibroblasts. *Biochem. Biophys. Res. Commun.* **2006**, *350*, 623–628.
70. Tanaka, M.; Sasaki, K.; Kamata, R.; Sakai, R. The C-terminus of Ephrin-B1 Regulates Metalloproteinase Secretion and Invasion of Cancer Cells. *J. Cell Sci.* **2007**, *120*, 2179–2189.
71. Lauffenburger, D. A.; Horwitz, A. F. Cell Migration: A Physically Integrated Molecular Process. *Cell* **1996**, *84*, 359–369.
72. Friedl, P.; Wolf, K. Tumour-Cell Invasion and Migration: Diversity and Escape Mechanisms. *Nat. Rev. Cancer* **2003**, *3*, 362–374.
73. Kim, J. S.; Granstrom, M.; Friend, R. H.; Johansson, N.; Salaneck, W. R.; Daik, R.; Feast, W. J.; Cacialli, F. Indium-tin Oxide Treatments for Single- and Double-layer Polymeric Light-emitting Diodes: The Relation between the Anode Physical, Chemical, and Morphological Properties and the Device Performance. *J. Appl. Phys.* **1998**, *84*, 6859–6870.